

# Multidimensional hydrodynamic simulations of the hydrogen injection flash

M. Mocák<sup>1</sup>, L. Siess<sup>1</sup> and E. Müller<sup>2</sup>

<sup>1</sup> Institut d'Astronomie et d'Astrophysique, Université Libre de Bruxelles, ULB - CP 226, 1050 Brussels, Belgium  
e-mail: mmocak@ulb.ac.be, siess@astro.ulb.ac.be

<sup>2</sup> Max-Planck-Institut für Astrophysik, Postfach 1312, 85741 Garching, Germany  
e-mail: ewald@mpa-garching.mpg.de

Received .....

## ABSTRACT

**Context.** The injection of hydrogen into the convection shell powered by helium burning during the core helium flash is commonly encountered during the evolution of metal-free and extremely metal-poor low-mass stars. Recent multidimensional hydrodynamic simulations indicate that the hydrogen injection may also occur in more metal-rich stars due to turbulent entrainment which accelerates the growth of the shell convection zone and increases its size. However, 1D stellar models cast doubts that helium-flash hydrogen mixing does occur as it requires the crossing of an entropy barrier at the helium-hydrogen interface.

**Aims.** With specifically designed multidimensional hydrodynamic simulations, we aim to prove that an entropy barrier is no obstacle for the growth of the helium-burning shell convection zone in the helium core of a metal-rich Pop I star, *i.e.*, convection can penetrate into the hydrogen-rich layers for these stars, too. We further study whether this is also possible in one-dimensional stellar evolutionary calculations

**Methods.** We artificially shift the hydrogen-rich layer closer to the outer edge of the helium-burning shell convection zone in a Pop I star with a mass of  $1.25 M_{\odot}$ , and simulate the subsequent evolution in 2D and 3D, respectively. We also perform stellar evolutionary calculations of the core helium flash in metal-rich stars implementing turbulent entrainment by means of a simple prescription. These simulations were performed with the Eulerian hydrodynamics code HERAKLES and the stellar evolution code STAREVOL, respectively.

**Results.** Our hydrodynamical simulations show that the helium-burning shell convection zone in the helium core moves across the entropy barrier and reaches the hydrogen-rich layers. This leads to mixing of protons into the hotter layers of the core and to a rapid increase of the nuclear energy production at the upper edge of the helium-burning convection shell - the hydrogen injection flash. As a result a second convection zone appears in the hydrogen-rich layers. Contrary to 1D models, the entropy barrier separating the two convective shells from each other is largely permeable to chemical transport when allowing for multidimensional flow, and consequently, hydrogen is continuously mixed deep into the helium core. We find it difficult to achieve such a behavior in one-dimensional stellar evolutionary calculations.

**Key words.** Stars: evolution – hydrodynamics – convection – hydrogen injection

## 1. Introduction

The hydrogen injection flash is believed to commence during the core helium flash of metal-free and extremely metal-poor (metallicity  $Z < 10^{-4}$ ) low-mass stars when their helium core shell convection zone penetrates into the hydrogen-rich layers (Fujimoto et al. 1990; Hollowell et al. 1990; Schlattl et al. 2001; Cassisi et al. 2003; Weiss et al. 2004; Campbell & Lattanzio 2008). Such an injection of protons is not expected for more metal-rich low-mass stars because the ignition of helium occurs further away from the hydrogen-rich layer and the entropy barrier between the helium and hydrogen layers is higher.

Multidimensional hydrodynamic simulations demonstrate that entropy barriers in stars are not as impenetrable as they may seem to be at first sight. The mixing beyond conventional Schwarzschild or Ledoux convection boundaries and the growth of convection zones on dynamic timescales due to turbulent entrainment are proves of it (Meakin & Arnett 2007). Recent hydrodynamic simulations of shell convection during the core helium flash also suggest that convection could reach the outer

hydrogen-rich layers of the star within a week <sup>1</sup> at around the peak of the core helium flash even in metal-rich stars (Mocák et al. 2009, 2010). However in these models, the hydrogen-rich layers are still far away from the helium-burning shell convection zone preventing the simulation of the expected proton injection process within an affordable amount of computing time. Alternatively, one may study the evolution during the core helium flash up to a possible hydrogen injection by one-dimensional stellar evolutionary calculations which include the effects of turbulent entrainment by means of a simple entrainment law. As such simulations are still missing, we implemented in our 1D stellar evolution code a simple entrainment law based on the ideas of Meakin & Arnett (2007), and performed stellar evolutionary calculations of the core helium flash in low-mass

<sup>1</sup> We find that the growth rate of the shell convection due to turbulent entrainment is of the order of a few meters per second for our hydrodynamic models, the exact value depending on the stability of the convection zone boundaries and the convective velocities near these boundaries (Meakin & Arnett 2007). The latter in turn depend not only on dimensionality of the flow (2D, 3D), but also on the spatial resolution of the simulation.

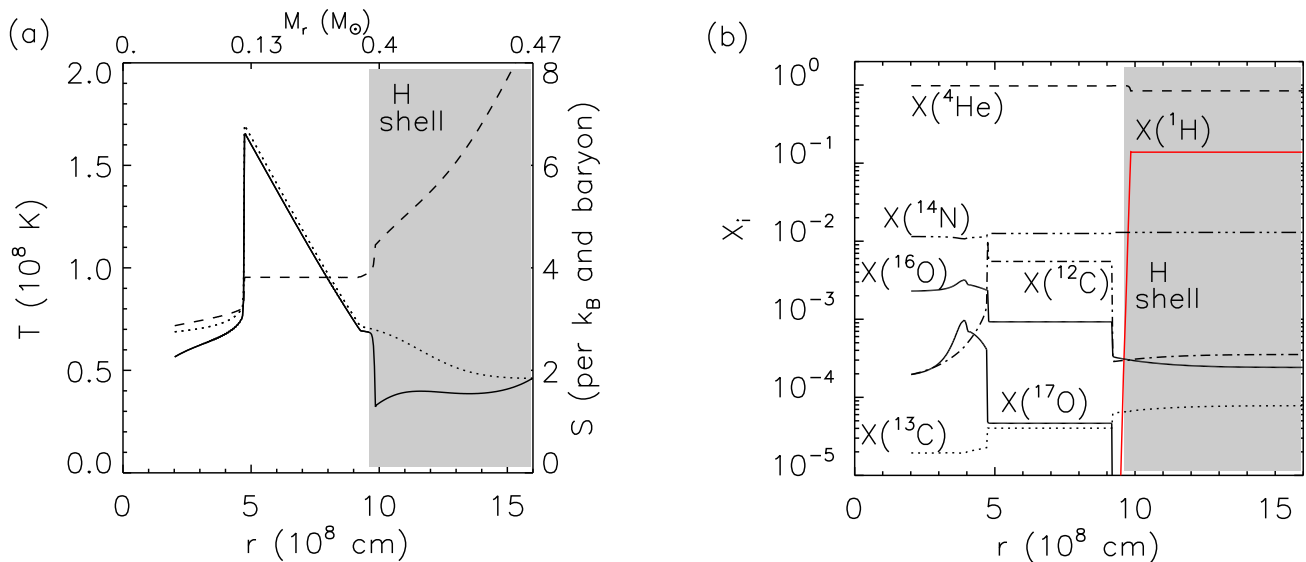


**Fig. 1.** (a; left panel): Temperature distribution of the modified initial model (MOD, solid) and of the original model (M, dotted) as a function of radius  $r$  and of enclosed mass  $M_r$  in solar units  $M_\odot$ , respectively. The dashed curve gives the entropy profile of model MOD. (b; right panel) Mass fraction of the main isotopes of model MOD as a function of radius. The hydrogen shell corresponds to the shaded region.

**Table 1.** Some properties of the modified initial stellar model MOD: Total mass  $M$ , mass  $M_{\text{He}}$  and radius  $R_{\text{He}}$  of the helium core, total nuclear energy production by helium burning  $L_{\text{He}}$ , and by hydrogen burning  $L_H^p$  and  $L_H^f$ , where the superscripts  $p$  and  $f$  denote that the respective numbers were obtained using a partial and full CNO network, respectively.

Model	$M$ [ $M_\odot$ ]	$M_{\text{He}}$ [ $M_\odot$ ]	$R_{\text{He}}$ [ $10^8$ cm]	$L_{\text{He}}$ [ $10^9 L_\odot$ ]	$L_H^p$ [ $10^9 L_\odot$ ]	$L_H^f$ [ $10^9 L_\odot$ ]
MOD	1.25	0.4	9.6	0.6	0.1	0.3

Pop I stars. The entrainment rates adopted for these calculations are taken from three-dimensional hydrodynamic simulations of Mocák et al. (2010).

Hydrodynamic simulations of similar phases of stellar evolution are currently also carried out by Herwig et al. (2006, 2011). The results of their and our studies can have important implications for the hydrogen injection not only during the core helium flash but also during the early-AGB phase (*i.e.*, the “dual shell flashes” described in Campbell & Lattanzio (2008)) or in more advanced nuclear burning stages.

The paper is organized as follows. We introduce the numerical tools and the stellar input model used for our simulations in the next section. The hydrodynamic simulations of the hydrogen injection phase and the stellar evolutionary calculations mimicking turbulent entrainment during the core helium flash are presented in Sect. 3, and Sect. 4, respectively. A summary of our findings is given in Sect. 5.

## 2. Physical Input and Codes

For the multidimensional hydrodynamic simulations we used the HERAKLES code (Mocák et al. 2008) derived from the PROMETHEUS code (Fryxell et al. 1991; Müller et al. 1991). In brief, HERAKLES solves the Euler equations coupled with source terms describing self-gravity and nuclear burning. The

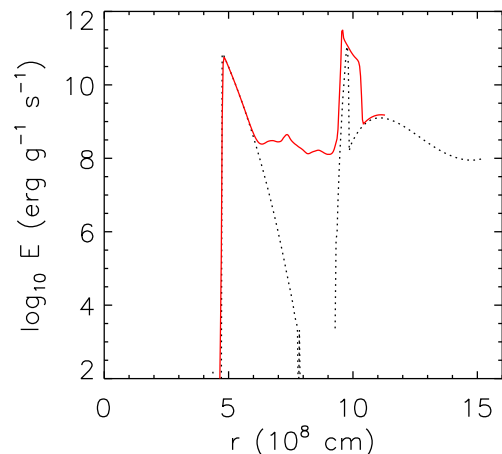


**Fig. 2.** Nuclear energy production rate as a function of radius  $r$  for the 3D model exp3if.3d.f at  $t = 0$  s (dotted-black), and at  $t = 9800$  s (solid-red), respectively.

hydrodynamic equations are integrated with the PPM reconstruction scheme (Colella & Woodward 1984) and a Riemann solver for real gases according to Colella & Glaz (1984). The evolution of the chemical species is described by a set of additional continuity equations (Plewa & Müller 1999). Self-gravity is handled according to Müller & Steinmetz (1995), gravitational potential being approximated by a 1D Newtonian potential obtained from the spherically averaged mass distribution. The code integrates nuclear networks with the semi-implicit Bader-Deufelhard method (Bader & Deufelhard 1983; Press et al. 1992).

As an initial model we used the helium core structure of a  $1.25 M_\odot$ ,  $Z = Z_\odot$  star during the core helium flash at its peak nuclear luminosity (Tab. 1). In the initial model, computed with the GARSTEC stellar evolution code (Weiss & Schlattl 2000,

**Table 2.** Some properties of the 2D and 3D hydrodynamic simulations based on model MOD: wedge size  $w$ ; number of grid points and resolution in  $r$ ,  $\theta$ , and  $\phi$  direction, respectively; estimated Reynolds number  $R_e$ ; characteristic velocity  $v_c$  of the convective flow in helium-burning layers; typical convective turnover timescale  $\tau_{conv}$  at time at  $t \sim 40\,000$  s for model 2d.p, and at  $t \sim 2500$  s for models 2d.f and 3d.f, respectively;  $t_{max}$  final evolutionary time.

run [name]	$w$ [°]	grid $N_r \times N_\theta \times N_\phi$	$\Delta r$ [ $10^6$ cm]	$\Delta \theta$ [°]	$\Delta \phi$ [°]	$R_e$	$v_c$ [ $10^6$ cm s $^{-1}$ ]	$\tau_{conv}$ [s]	$t_{max}$ [s]
hifexp.3d.f	45	$370 \times 45 \times 45$	3.8	1	1	$10^2$	1.0	1000	14400
hifexp.2d.f	90	$370 \times 90$	3.8	1	-	$10^2$	1.7	600	14400
hifexp.2d.p	90	$370 \times 90$	3.8	1	-	$10^2$	1.8	550	200000

2007), the hydrogen-rich layers are artificially shifted closer to the outer boundary of the helium-burning shell convection zone at radius around  $9.8 \times 10^8$  cm. Originally the lower boundary of the hydrogen layer is located at a radius of  $1.9 \times 10^9$  cm. The unmodified initial model (M) is described in more detail in Mocák et al. (2008, 2009). Compared to this model the resulting hydrostatic structure of the modified initial model MOD differs by a temperature sink at the boundary between the helium and hydrogen-rich layers (H-He boundary) at  $9.5 \times 10^8$  cm  $< r < 10 \times 10^8$  cm (Fig. 1). At this boundary the entropy increases almost discontinuously by 20%, producing the so-called barrier. The temperature gradient in the helium-burning convection zone ( $4.7 \times 10^8$  cm  $< r < 9.2 \times 10^8$  cm) remains almost unaltered as well as the nuclear energy production.

At the H-He boundary of model MOD around  $r \sim 9.8 \times 10^8$  cm, we find a narrow peak in the nuclear energy production rate (Fig. 2) that is due to some left-over hydrogen ( $X \sim 10^{-4}$ ) when modifying the original initial model. In the layers near the H-He boundary the temperature is relatively high ( $T \sim 5 \times 10^7$  K), and even if the hydrogen mass fraction is small, the nuclear energy production is significant. Although, this feature is not seen in 1D stellar evolution simulations of the hydrogen injection flash (Hollowell et al. 1990), it may represent a somewhat more “realistic” situation, where the H-He interface is not a discontinuity but a moderately hot layer partially enriched with hydrogen.

For the stellar evolutionary calculations of the core helium flash we implemented a simple turbulent entrainment law in the STAREVOL code (Siess 2006) and evolved a  $1 M_\odot$ ,  $Z = Z_\odot$  star for different entrainment rates guided by our 3D hydrodynamic simulations. To achieve hydrogen injection even in metal-rich low-mass stars, we also tried the classical overshooting prescription based on the exponential decay of the convective velocity field beyond the convection zone boundaries (Freytag et al. 1996) with various efficiencies.

STAREVOL is a 1D lagrangian stellar evolution code able to compute the evolution of stars in the mass range (0.1 - 60  $M_\odot$ ) from pre-main sequence up to Neon ignition. The nuclear network includes 53 species coupled by 177 nuclear reactions (Siess & Arnould 2008), an accurate equation of state tested in the domain of very low mass stars (Siess et al. 2000), and all relevant neutrino contributions (for a detailed description, the reader is referred to Siess (2006)). This code has been widely used to study pre-main sequence stars (Siess et al. 1997), rotational mixing (Palacios et al. 2006), AGB nucleosynthesis (Siess et al. 2002) and super AGB stars (Siess 2010).

### 3. Hydrodynamic simulations

We performed two 2D (models hifexp.2d.f and hifexp.2d.p) and one 3D (model hifexp.3d.f) hydrodynamic simulation using dif-

ferent nuclear reaction networks. The last letter of the model name,  $f$  and  $p$ , refers to simulations performed with a full and partial CNO reaction network (*i.e.*, neglecting reactions related to  $^{13}\text{N}$  and  $^{15}\text{O}$ ). These runs start from the modified initial model MOD with the shifted hydrogen profile. Some general properties of these simulations are summarized in the Tab. 2, all of which were performed on an equidistant spherical grid ranging in radius from  $2 \times 10^8$  cm to  $1.6 \times 10^9$  cm. The adopted grid resolution is motivated by our earlier work (Mocák et al. 2008), where we found convergence of the results starting at a radial grid resolution  $\Delta r \sim 3.7 \times 10^6$  cm and an angular resolution of  $\sim 1^\circ$ . The boundary conditions in the radial direction are reflective, while periodic boundaries are imposed in the angular directions. For models hifexp.3d.f and hifexp.2d.f the reaction network includes the following species:  $^1\text{H}$ ,  $^3\text{He}$ ,  $^4\text{He}$ ,  $^{12}\text{C}$ ,  $^{13}\text{C}$ ,  $^{13}\text{N}$ ,  $^{14}\text{N}$ ,  $^{15}\text{N}$ ,  $^{15}\text{O}$ ,  $^{16}\text{O}$ ,  $^{17}\text{O}$ ,  $^{20}\text{Ne}$ ,  $^{24}\text{Mg}$ , and  $^{28}\text{Si}$ , coupled by reactions of the full CNO cycle and the triple- $\alpha$  reaction. More details are given in the PhD thesis of Mocák (2009).

For the simulation hifexp.2d.p we omitted the isotopes  $^{13}\text{N}$  and  $^{15}\text{O}$ , the  $\beta$ -decay reactions of the CNO cycle and the  $^{12}\text{C}(p,\gamma)^{13}\text{N}$  reaction. Although this variant is unrealistic, it allows us to demonstrate that entropy barriers which are not sustained by sufficiently strong nuclear burning can be completely destroyed by the growing convection zone due to turbulent entrainment. When considering all species of the full CNO cycle, the nuclear energy production at the H-He boundary is a factor of 3 higher than in the partial network and leads to the formation of a shell convection zone in the hydrogen-rich layers (Fig. 3; models hifexp.2d.f and hifexp.3d.f; see Sect. 3.1). No shell convection zone appears in the hydrogen-rich layers of the 2D model hifexp.2d.p.

#### 3.1. Simulations with the full CNO reaction network

Our hydrodynamic 3D and 2D models, hifexp.3d.f and hifexp.2d.f (Fig. 3), are evolved with an accurate treatment of the CNO cycle on a numerical grid having the same number of zones in radial and angular directions. The latter allows us to compare the results of these simulations being biased only by the dimensionality of the simulation, but not by the grid resolution.

In the 3D (2D) model, hifexp.3d.f (hifexp.2d.f), after 800 s (1000 s) convection fully develops in the layers located above the temperature maximum  $T_{max}$  ( $r \sim 4.7 \times 10^8$  cm). As soon as the first convective plumes reach the H-He boundary, the dredge-down of hydrogen sets in. Up to  $\sim 1500$  s the composition profile in both models is similar, with a steep increase of the hydrogen mass fraction  $X(^1\text{H})$  exceeding  $10^{-9}$  just below the H-He interface (Fig. 4). Subsequently and until  $t \sim 8000$  s,  $X(^1\text{H})$  remains almost constant in the helium-burning convection zone of the 3D model, where  $10^{-10} < X(^1\text{H}) < 10^{-8}$ . This is in contrast with the 2D simulation, hifexp.2d.f, where  $X(^1\text{H})$  continues to

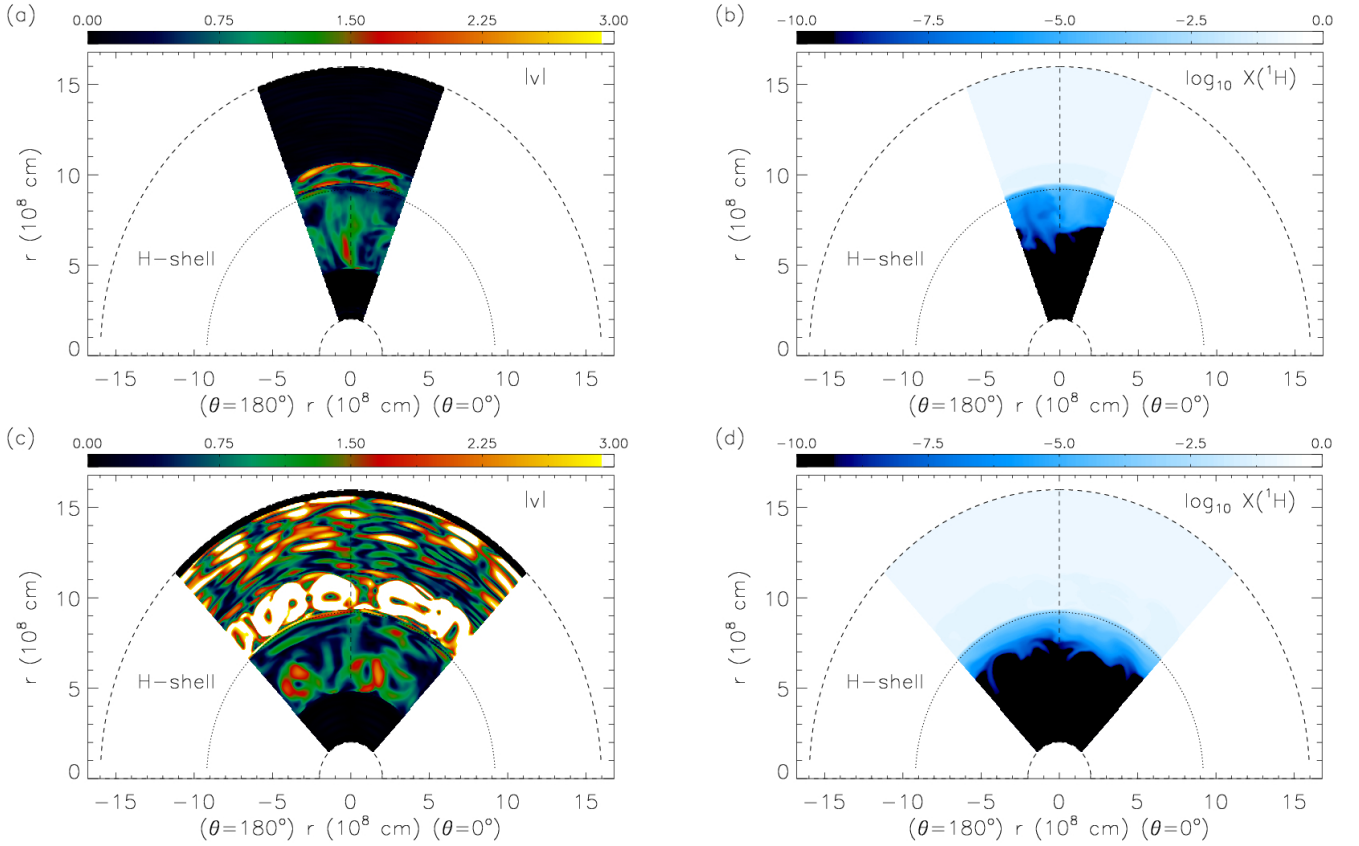


**Fig. 3.** Top row: snapshots showing contour plots of the modulus of the velocity  $|v|$  (in units of  $10^6 \text{ cm s}^{-1}$ ; left panel) and the hydrogen mass fraction (right panel) for the 3D model hifexp.3d.f at  $t \sim 13300 \text{ s}$  in the meridional plane ( $\phi = 0^\circ$ ). Bottom row: same quantities but for the 2D model hifexp.2d.f. The dotted line separates helium- and hydrogen-rich layers (H-shell), and the dashed lines mark the boundaries of the computational domain.

increase during this epoch. Between 8000 s and 12 000 s, the proton mass fraction increases in the helium-burning convection of both 2D and 3D models.

At  $t \sim 12 000 \text{ s}$ , the entropy barrier at the H-He interface in both models is steeper and almost twice as large as it was at the beginning of the simulations due to the enhanced nuclear burning. This increase in temperature and entropy at the interface slows down the injection of protons and the hydrogen mass fraction in the helium-rich layers decreases (Fig. 4).

As protons are dredged down into the helium core, they are captured by  $^{12}\text{C}$  via the  $^{12}\text{C}(p, \gamma)^{13}\text{N}$  reaction, *i.e.*, the hydrogen abundance decreases sharply with depth. Nevertheless, some protons can reach layers with temperatures exceeding  $10^8 \text{ K}$ , where their lifetime against the  $^{12}\text{C}(p, \gamma)^{13}\text{N}$  reaction is  $\lesssim 100 \text{ s}$  (Caughlan & Fowler 1988). This is much shorter than their lifetime outside the He-burning convection shell. As the convective plumes have velocities of  $10^6 \text{ cm s}^{-1}$  ( $2 \times 10^6 \text{ cm s}^{-1}$ ) in the 3D (2D) model, hydrogen-rich gas is advected from the “colder” top of the He-burning convection shell to the aforementioned hot layers (located at  $r \sim 7.7 \times 10^8 \text{ cm s}^{-1}$ ) in less than 200 s (100 s). Our simulations show that this time is too short for the hydrogen to burn completely while being advected to layers with temperatures  $\gtrsim 10^8 \text{ K}$  (Fig. 4).

The differences between the  $X(^1\text{H})$  distributions of the 2D and 3D model can be understood by realizing that the convective velocities in the 3D model are almost a factor of two smaller than in the 2D one. Hence, there is more time for hydrogen to burn during its transport in the 3D model than in the 2D one, *i.e.*, hydrogen is able to reach the hot layers in larger amounts

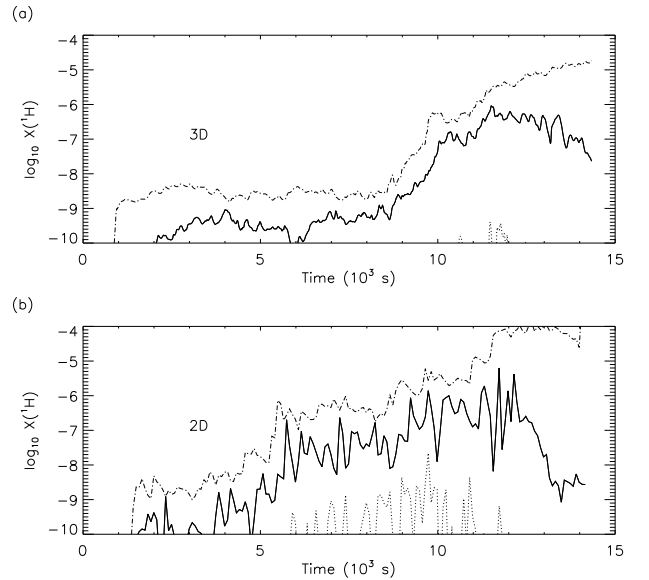


**Fig. 4.** Temporal evolution of the (logarithm of the) hydrogen mass fraction  $X(^1\text{H})$  at three different radii [temperatures] around the top, middle, and bottom of the helium-burning convection shell, respectively:  $r_1 = 8.8 \times 10^8 \text{ cm}$  [ $T_1 \sim 0.8 \times 10^8 \text{ K}$ ] (dash-dotted),  $r_2 = 7.1 \times 10^8 \text{ cm}$  [ $T_2 \sim 1.2 \times 10^8 \text{ K}$ ] (solid), and  $r_3 = 5.4 \times 10^8 \text{ cm}$  [ $T_3 \sim 1.5 \times 10^8 \text{ K}$ ] (dotted). The upper panel (a) gives the results for the 3D model hifexp.3d.f, and the lower panel (b) for the 2D model hifexp.2d.f, respectively.



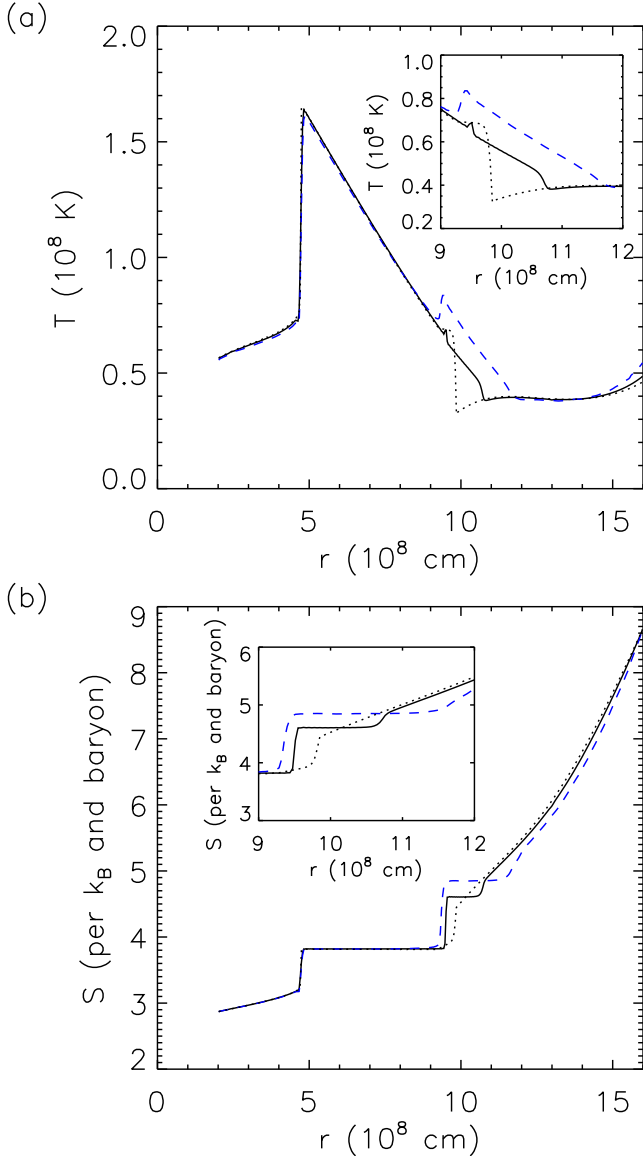


**Fig. 5.** Radial distribution of (a) temperature and (b) entropy at  $t = 0$  s (dotted) and  $t_1 = 13\,500$  s for the 2D model hifexp.2d.f (dashed, blue), and the 3D model hifexp.3d.f (solid), respectively. The inserts show a zoom of the region around the H-He interface.

in the latter case (Fig. 4). Besides higher convective velocities, the convective plumes arising at the H-He boundary also fill a larger volume fraction in the 2D model compared with the 3D one, where the plumes are smaller and narrower.

The nuclear energy production at the H-He boundary and the impacting convective plumes change the initial properties of the H-He interface. At the start of the simulations, the boundary is characterized by a steep radial step in both the temperature and entropy profiles. However, when convection reaches the interface, the single step structure of the temperature and entropy profiles evolves into a two steps structure exhibiting a narrow entropy plateau between the steps (Fig. 5). This plateau reflects the formation of a secondary convection shell, located in the hydrogen-rich layers and powered by the CNO cycle. We find higher absolute values of both the entropy and temperature in the 2D model, hifexp.2d.f, compared to its 3D counterpart across the forming new convection shell. This can be explained

by the stronger nuclear burning occurring in that model, which also leads to a faster growth of the hydrogen-burning convection shell.

Nuclear burning at the H-He interface steadily increases during both simulations, and eventually leads to the formation of a distinct second temperature peak (Fig. 5, Fig. 7). This behavior is well known from 1D stellar evolutionary calculations of the core helium flash in extremely metal-poor stars, where the helium-burning convection shell splits after the injection of hydrogen. However, the splitting process seen in 1D stellar calculations differs from that found in our multidimensional simulations. In 1D simulations the splitting occurs due to the appearance of a temperature peak in the convective helium-burning shell at the location where hydrogen burning by the  $^{12}\text{C}(\text{p}, \gamma)^{13}\text{N}$  reaction is proceeding the fastest.

In our hydrodynamic models the appearance of a second temperature peak is preceded by a slow migration of the H-He boundary into the helium-burning convective shell, which forces it to retreat slightly (Fig. 7). Eventually, when the nuclear energy release and the temperature at the H-He boundary become sufficiently high, we observe the appearance of a new convection shell in the hydrogen-rich layers above the original one. Hence, what actually happens is not a splitting, but a “retreat” of the initial helium-burning convection shell and the birth of a new one on top of it powered by burning of hydrogen.

Our hydrodynamic simulations exhibit another major distinct property: the absence of an impermeable radiative layer between the two convective shells. Mixing of nuclear species between these layers is not prohibited, but occurs during the whole event (Fig. 6) with a decreasing efficiency towards the end of simulation.

The evolution of the hydrodynamic models is likely representative of early phases during the dual core and He-shell flashes, and indicates that the entropy barrier does not inhibit hydrogen dredge-down. However, this conclusion should be moderated by the fact that the entropy at the H-He boundary can increase by the rise of the nuclear energy production. Eventually, this entropy barrier may become so high that mixing ceases completely. What we have shown here is that, given our initial conditions, nothing seems to prevent H-injection, at least in the early stages. A similar behavior was also found by Herwig et al. (2011) in their 3D simulations of the hydrogen injection into the helium shell flash convection zone which helped them to explain major features observed in spectra of the Sakurai’s object (Duerbeck et al. 2000) (post-AGB object experiencing its last helium flash). Finally note that proton injection may have interesting consequences concerning the production of s-process elements as some  $^{13}\text{C}$  can be produced which is a source of neutrons (Campbell et al. 2010).

We note, that during its final evolution the 2D model hifexp.2d.f eventually experiences another unrealistic nuclear runaway when He ignites in the secondary convection shell (due to high temperature  $\gtrsim 10^8$  K at the H-He boundary) causing it to rapidly expand to the outer boundary of the computational domain, when we stopped the calculation (Fig. 6 b). Concerning this unexpected behavior we have to emphasize that these hydrodynamical simulations are strongly dependent on the initial conditions. In particular, we note that in the initial model MOD the layers at the H-He boundary are highly degenerate (degeneracy parameter  $\psi \approx 10$ ).<sup>2</sup> Such a large degeneracy favors a nuclear runaway. Additionally, our multidimensional simulations

<sup>2</sup> Matter at the H-He boundary after proton injection (and some earlier expansion) in a 1D population III model of  $0.85 M_{\odot}$  computed by

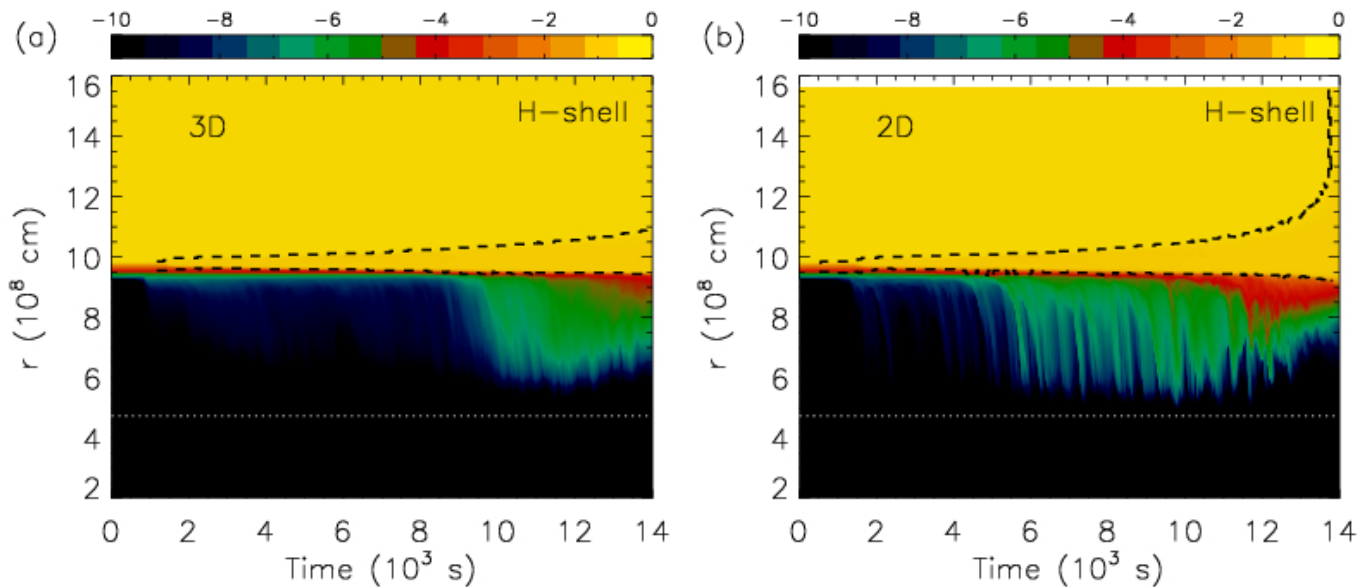


**Fig. 6.** (a) Temporal evolution of the angle-averaged radial distribution of (the logarithm of) the hydrogen mass fraction for the 3D model hifexp.3d.f, and (b) for the 2D model hifexp.2d.f, respectively. The dashed lines delineate the boundaries of the newly forming hydrogen-burning convection shell, and the dotted line marks the bottom of the helium-burning convection zone.

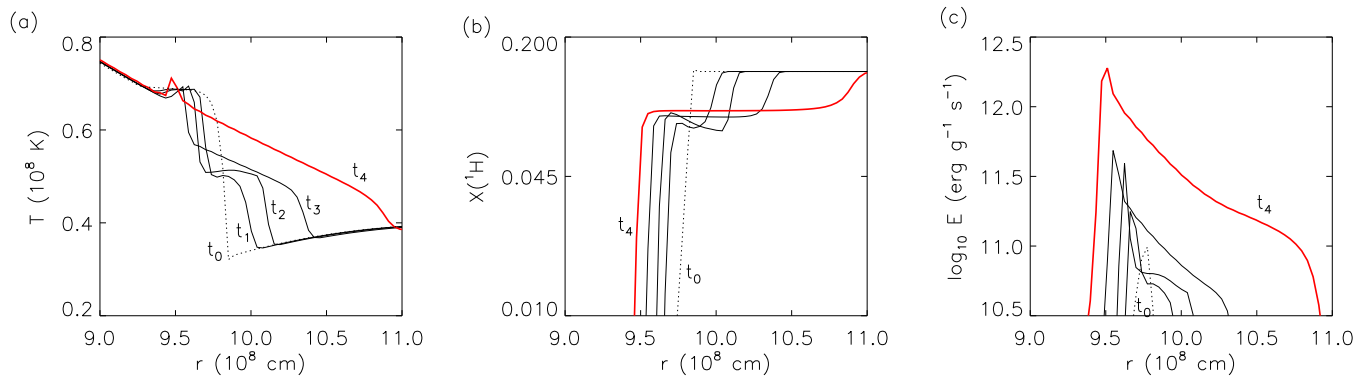


**Fig. 7.** Radial distribution of (a) temperature, (b) hydrogen mass fraction, and (c) energy production rate at the H-He interface for the 3D model hifexp.3d.f at five different times:  $t_0 = 0$  s,  $t_1 = 3230$  s,  $t_2 = 6500$  s,  $t_3 = 10\,400$  s, and  $t_4 = 14\,340$  s.

are likely to underestimate the star's expansion and subsequent cooling because of the reflective boundary conditions imposed in the radial direction. These numerical restrictions limit the cooling and favor the aforementioned helium runaway.

### 3.2. Simulation with partial CNO network

In the 2D simulation hifexp.2d.p we did neither consider the  $\beta$ -decay reactions  $^{13}\text{N}(\beta^-)^{13}\text{C}$  and  $^{15}\text{O}(\beta^-)^{15}\text{N}$ , nor the  $^{12}\text{C}(p, \gamma)^{13}\text{N}$  reaction, which gives rise to a reduced energy production rate by roughly a factor of three at the H-He interface. It allowed us to demonstrate, that entropy barriers at convection zone boundaries that are insufficiently sustained by nuclear burning are penetrable and unable to prevent the growth of the convection zone due to turbulent entrainment on dynamic timescales. By neglecting proton capture on  $^{12}\text{C}$  in the simulation, we obtain an incorrect hydrogen profile and a reduced nuclear energy production rate. That explains why we do not

observe here the formation of the secondary hydrogen-burning shell convection as in our hydrodynamic models with the full nuclear CNO reaction network (see previous subsection).

In this model, helium-burning convection starts at  $t \sim 1000$  s and extends throughout the whole initially convectively unstable shell as determined by the Schwarzschild criterion. The convection shell is located between the radius of the temperature maximum and the base of the hydrogen-rich layers. It is characterized by vortices, which are typical structures of 2D simulations due to the imposed axial symmetry. Their width is equal to the radial extent of the convection shell, *i.e.*,  $r \sim 5 \times 10^8$  cm, which is also the width of the convection zone in the unmodified initial model (M).

The shell convection reaches the hydrogen-rich layers shortly after the appearance of the first convective plumes. It initiates the dredge-down of protons deep into the helium core, and causes the outer boundary of the convection shell to cross the entropy barrier at the H-He interface (Fig. 8). The value of the entropy at this interface constantly decreases due to turbulent entrainment, which effectively shifts the entropy barrier to larger radii.

Simon Campbell (private communication) (Mocák 2009) has a degeneracy parameter  $\psi \approx -2$ .

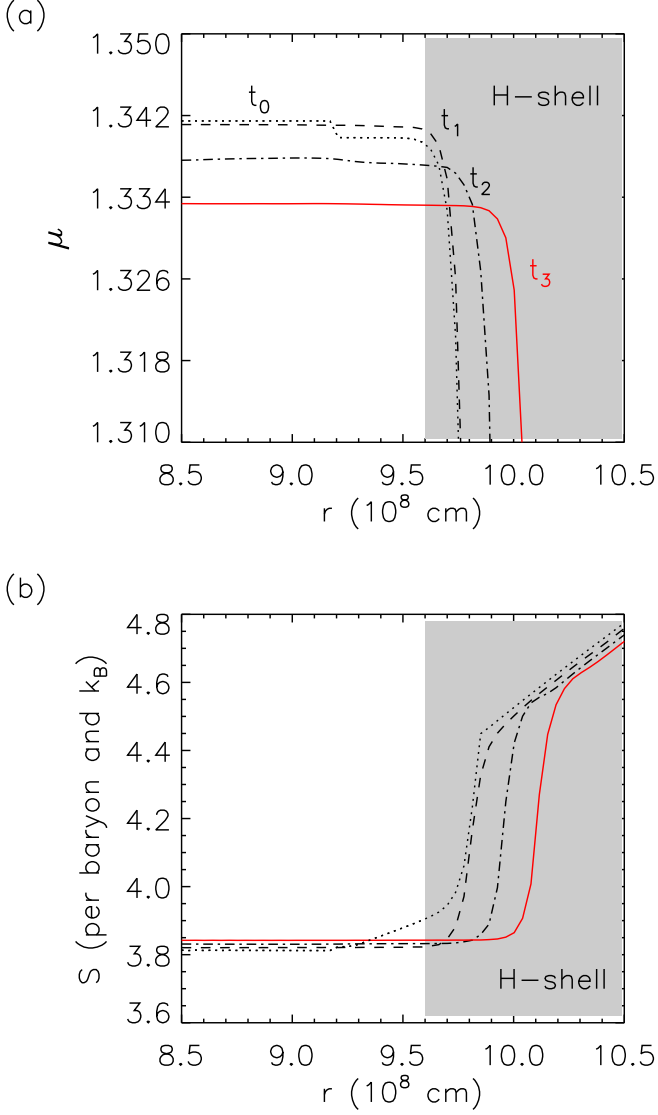


**Fig. 8.** Mean molecular weight (a) and entropy (b) at the outer edge of the convection zone of the 2D model simulated with the partial CNO network (hifexp.2d.p) at four different times:  $t_0 = 0$  s (dotted),  $t_1 = 46\,600$  s (dashed),  $t_2 = 94\,200$  s (dash-dotted), and  $t_3 = 142\,000$  s (solid red).

The entrainment rate of the outer convection boundary is initially relatively high, around  $70 \text{ m s}^{-1}$ , but after roughly  $30\,000$  s it drops and eventually relaxes to an almost constant value of  $\sim 4.5 \text{ m s}^{-1}$ . The entropy barrier has a stabilizing effect because it decreases the entrainment velocity. However, it does not prevent the advance of the convection zone into the H-rich layers and leads to an erosion of the entropy gradient. After  $170\,000$  s the shell convection has moved  $\sim 8 \times 10^7$  cm into the H-rich buffer, meaning that almost 12% of the hydrogen-rich shell included into the simulation (limited by the outer radial grid boundary at  $1.6 \times 10^9$  cm) is already entrained within only 47 hours, or  $\sim 300$  convective turnover timescales.

In this simulation, protons are able to reach layers with temperatures as high as  $\sim 1.8 \times 10^8$  K. However, such a deep mixing of hydrogen into the helium burning layers is not realistic because protons should have been captured by  $^{12}\text{C}$  before.

#### 4. Stellar evolutionary calculations

To mimic the effects of the turbulent entrainment in 1D stellar evolutionary calculations, we experiment and implement a simple entrainment law

$$\dot{M}_E = \frac{\partial M}{\partial r} u_E \quad (1)$$

where  $M$  is the mass of the shell at radius  $r$  and  $u_E$  is the entrainment rate (Meakin & Arnett 2007). We simulated a  $1 M_\odot$ ,  $Z = Z_\odot$  star up to the core helium flash. At first we use an entrainment rate of  $6.7 \times 10^2 \text{ cm s}^{-1}$  as found by Mocák et al. (2009) in their 3D hydrodynamic simulations of the core helium flash. The entrainment is switched on only shortly before the flash reaches its maximum intensity (maximum nuclear energy generated in the helium core). We find that the He-convection zone boundary is unable to cross the entropy barrier and penetrate into the hydrogen shell. This result also holds when increasing the entrainment rate by one or even two orders of magnitude.

This is partially due to the inherent time dependence of the mixing prescription. Indeed, for a given timestep  $\Delta t$ , mixing will extend over a mass range given by  $\Delta M_e = \dot{M}_E \Delta t$ . Practically, we simply shift the convective boundary to the new mass location  $M_{\text{conv}}^{\text{edge}} + \Delta M_e$ . As the helium convection shell approaches the H-rich layer, the timestep which is constrained among other things by the rate of change of the nuclear luminosity, decreases thus preventing the injection of protons and a subsequent H-flash. Eventually, a (small) timestep is found that allows the simulation to go on and after the some time, the helium-shell convection zone naturally quenches and H-injection is avoided.

On the other hand, if we experiment with overshooting by using the exponential decay of the convection velocity in the radiative layers, mixing is treated as a diffusive process with the diffusion coefficient given by

$$D_{\text{over}} = D_{\text{conv}} \exp(-|r - r_{\text{edge}}|/(2fH_P)) \quad (2)$$

where  $H_P$  is the pressure scale height at the edge of the convective zone and  $f$  a free parameter. Compared to the previous prescription, this treatment shows two main differences: mixing is treated as a diffusive process so the penetration of the H-shell convection is “smoother” and the new convective boundary at  $t + \Delta t$  does not explicitly depend on its location at time  $t$  and on the timestep. Our 1D experiments indicate that at solar metallicity, a substantial overshooting is required to trigger an injection with  $f \sim 1$ . This injection then leads to the splitting of the He-shell convection and after some structural readjustment to the pollution of the envelope. We report C and N enrichments by a factor of 2 or 3. Interestingly, we find that subsequently to this mixing event, the  $^{12}\text{C}/^{13}\text{C}$  ratio has dropped to below  $\sim 10$ . Moreover, these He-core burning stars are carbon-rich ( $\text{C/O} \sim 1.7$ ) and show large  $^7\text{Li}$  abundances ( $\varepsilon(\text{Li}) \approx 3.5$ ). Some of these features are found in J-stars but contrarily to observations, our models show a too large  $^{16}\text{O}/^{17}\text{O}$  ratio (by a factor of two at least, and the C/N ratio is too low in our models).

#### 5. Summary

We performed hydrodynamic simulations of shell convection in the core of a low mass star at the peak luminosity of the helium flash. In these computations, the hydrogen-rich layers were artificially shifted down into the helium core. They allowed us to demonstrate a penetration of the helium-burning shell convection into the hydrogen layers due to turbulent entrainment despite the presence of an entropy barrier between them. Resulting consequences are the following.

Hydrodynamic models computed with the full CNO reaction network leads to the formation of a secondary shell convection zone in the hydrogen-rich layers. It is powered by hydrogen burning and is located above the already-present helium-burning shell convection. These simulations show (contrary to 1D stellar calculations of similar evolutionary phases) that the mixing of protons down to the helium-burning convection shell is not completely inhibited, although it eventually slows down due to an increase of the nuclear energy production and the growth of the entropy barrier at the interface between the helium-burning and hydrogen-burning convection shell.

In our hydrodynamic model computed with a reduced nuclear reaction network the energy production rate in the hydrogen-rich layers is smaller and we do not observe an appearance of the hydrogen-burning convection shell. This simulation shows, that an entropy barrier not sustained sufficiently by nuclear burning does not act as an obstacle for the growing helium-burning convection shell due to turbulent entrainment. The entrainment rate of the outer rim of the helium-burning convection zone reaches a roughly constant non-vanishing value.

Given our initial model of low-mass and metal-rich star, the aforementioned situations were difficult to reconstruct by one-dimensional stellar evolution code.

*Acknowledgements.* The simulations were performed at the Rechenzentrum Garching on the IBM Power6 system. The authors want to thank Frank Timmes for some of his publicly available FORTRAN subroutines which we used in the HERAKLES code. Miroslav Mocák acknowledges financial support from the Communauté française de Belgique - Actions de Recherche Concertées. LS is FNRS research associate. We also thank John Lattanzio for summarizing the observations about J-stars.

## References

- Bader, G. & Deuffhard, P. 1983, *Numer. Math.*, 41, 373  
 Campbell, S. W. & Lattanzio, J. C. 2008, *A&A*, 490, 769  
 Campbell, S. W., Lugaro, M., & Karakas, A. I. 2010, *A&A*, 522, L6+  
 Cassisi, S., Schlattl, H., Salaris, M., & Weiss, A. 2003, *ApJ*, 582, L43  
 Caughlan, G. R. & Fowler, W. A. 1988, *Atomic Data and Nuclear Data Tables*, 40, 283  
 Colella, P. & Glaz, H. H. 1984, *J.Comput.Phys.*, 59, 264  
 Colella, P. & Woodward, P. R. 1984, *J.Comput.Phys.*, 54, 174  
 Duerbeck, H. W., Liller, W., Sterken, C., et al. 2000, *AJ*, 119, 2360  
 Freytag, B., Ludwig, H., & Steffen, M. 1996, *A&A*, 313, 497  
 Fryxell, B., Arnett, D., & Müller, E. 1991, *ApJ*, 367, 619  
 Fujimoto, M. Y., Iben, I. J., & Hollowell, D. 1990, *ApJ*, 349, 580  
 Herwig, F., Freytag, B., Hueckstaedt, R. M., & Timmes, F. X. 2006, *ApJ*, 642, 1057  
 Herwig, F., Pignatari, M., Woodward, P. R., et al. 2011, *ApJ*, 727, 89  
 Hollowell, D., Iben, I. J., & Fujimoto, M. Y. 1990, *ApJ*, 351, 245  
 Meakin, C. A. & Arnett, D. 2007, *ApJ*, 667, 448  
 Mocák, M. 2009, PhD thesis, Max-Planck-Institut für Astrophysik, Garching bei München  
 Mocák, M., Campbell, S. W., Müller, E., & Kifonidis, K. 2010, *A&A*, 520, A114+  
 Mocák, M., Müller, E., Weiss, A., & Kifonidis, K. 2008, *A&A*, 490, 265  
 Mocák, M., Müller, E., Weiss, A., & Kifonidis, K. 2009, *A&A*, 501, 659  
 Müller, E., Fryxell, B., & Arnett, D. 1991, in *ESO/EIPC Workshop on Supernova 1987A and other Supernovae*, p. 99 - 116, 99–116  
 Müller, E. & Steinmetz, M. 1995, *Comp.Phys.Commun.*, 89, 45  
 Palacios, A., Charbonnel, C., Talon, S., & Siess, L. 2006, *A&A*, 453, 261  
 Plewa, T. & Müller, E. 1999, *A&A*, 342, 179  
 Press, W. H., Teukolsky, S. A., Vetterling, W. T., & P., F. B. 1992, in *Numerical Recipes in FORTRAN, The Art of Scientific Computing, Second Edition* (Cambridge: Cambridge University Press), Vol. 1  
 Schlattl, H., Cassisi, S., Salaris, M., & Weiss, A. 2001, *ApJ*, 559, 1082  
 Siess, L. 2006, *A&A*, 448, 717  
 Siess, L. 2010, *A&A*, 512, A10+  
 Siess, L. & Arnould, M. 2008, *A&A*, 489, 395  
 Siess, L., Dufour, E., & Forestini, M. 2000, *A&A*, 358, 593  
 Siess, L., Forestini, M., & Dougados, C. 1997, *A&A*, 324, 556  
 Siess, L., Livio, M., & Lattanzio, J. 2002, *ApJ*, 570, 329  
 Weiss, A. & Schlattl, H. 2000, *A&AS*, 144, 487  
 Weiss, A. & Schlattl, H. 2007, *Ap&SS*, 341  
 Weiss, A., Schlattl, H., Salaris, M., & Cassisi, S. 2004, *A&A*, 422, 217